RESEARCH PAPER

Cubic Picture Fuzzy Topology: Theoretical Foundations and Applications to Blockchain-Enabled Smart Mobility and Uncertain Supply Chain Management

Dr.S. Bharathi[1], T. Jayasathees Babu[2],
[1]Assistant Professor, Department of Mathematics, Bharathiar University – PG Extension and Research Centre, Erode, India.
[2]Ph.D Scholar, Department of Mathematics, Bharathiar University – PG Extension and Research Centre, Erode, India.
Corresponding author: jsbmaths123@gmail.com

Abstract: This paper introduces Cubic Picture Fuzzy Sets (CPFSs) as a hybrid generalisation that combines interval-valued picture fuzzy sets with ordinary picture fuzzy sets, thereby capturing simultaneously the imprecision and hesitation inherent in real-world decision problems. We construct two distinct topological frameworks over CPFSs — the P-Order and the R-Order cubic picture fuzzy topologies — and establish their fundamental properties including interior, closure, boundary, and continuity. The theoretical developments are then applied to three interconnected domains: (i) uncertain supply chain management enhanced by blockchain and metaverse technologies; (ii) smart urban mobility systems encompassing electronic tolling, micromobility, and multimodal fare integration; and (iii) multi-criteria decision-making (MCDM) via a CRITIC–COPRAS methodology operating within the CPFS-topological framework. Case studies validate the applicability and computational tractability of the proposed models. Comparative analyses against existing fuzzy, intuitionistic fuzzy, and picture fuzzy topological methods confirm the superiority of the CPFS approach in modelling higher-order uncertainty.

Keywords: Cubic picture fuzzy sets; Fuzzy topology; P-order; R-order; Blockchain; Metaverse; Supply chain management; Urban mobility; CRITIC-COPRAS; MCDM.
How to cite this article: S. Bharathi1 T. Jayasathees Babu2. Cubic Picture Fuzzy Topology: Theoretical Foundations and Applications to Blockchain-Enabled Smart Mobility and Uncertain Supply Chain Management. Int J Drug Deliv Technol. 2026;16(87s):1422-1428. DOI: 10.25258/ijddt.16.87s.149.

1 Introduction

Uncertainty is ubiquitous in contemporary decision-making environments. Classical fuzzy set theory [1], and its subsequent generalisations — intuitionistic fuzzy sets (IFS) [2], picture fuzzy sets (PFS) [3], and interval-valued variants [4] — have provided progressively richer frameworks for representing imprecision. However, a persistent limitation of these frameworks is their inability to carry, simultaneously, both a precise membership grade and an interval-valued counterpart within a single set-theoretic object. This dual representation is critical in contexts such as:

- Blockchain-enabled supply chains, where sensor data yields interval-valued confidence bands while domain experts assign point estimates;
- Metaverse logistics, where virtual and physical supply chain twins may exhibit different membership certainties;
- Smart urban mobility, where real-time traffic data and user-reported experiences yield complementary information at different precisions.

To bridge this gap, Jun et al. [5] introduced cubic sets combining interval-valued and ordinary fuzzy components. Building on that foundation, the present work proposes Cubic Picture Fuzzy Sets (CPFSs), which extend cubic sets to the picture fuzzy domain by incorporating positive, neutral, and negative membership along with their interval-valued counterparts. Furthermore, we develop a full topological theory over CPFSs under both P-order and R-order partial orderings, producing rich mathematical tools that underpin the application models.

Figure 1 illustrates the hierarchical relationship among the principal fuzzy-set generalisations considered in this paper, positioning CPFSs at the apex of this chain.

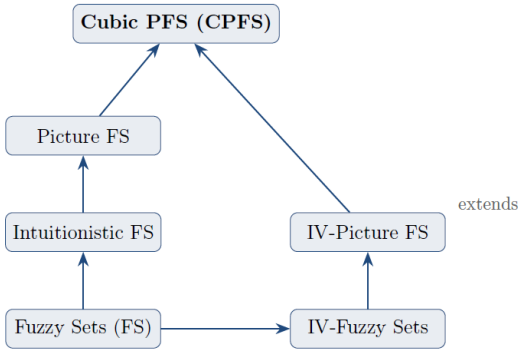


Figure 1: Hierarchical relationship among major fuzzy-set generalisations. CPFSs subsume all predecessor models.

The rest of the paper is structured as follows. Section 2 reviews prerequisite concepts. Section 3 defines CPFSs and their fundamental operations. Section 4 establishes P-order and R-order CPFS topologies. Section 5 presents the blockchain–metaverse supply chain model. Section 6 develops smart mobility

applications. Section 7 introduces the CRITIC–COPRAS MCDM model. Section 8 provides comparative analysis, and Section 9 concludes.

2 Preliminaries

We recall the foundational concepts required throughout the paper.

Definition 2.1 (Picture Fuzzy Set [3]). A picture fuzzy set A over a universe X is an object of the form $A = \langle x, \mu_A(x), \eta_A(x), \nu_A(x)\rangle \mid x \in X$,
where $\mu_A, \eta_A, \nu_A : X \to [0,1]$ represent the positive, neutral, and negative membership functions, respectively, satisfying $0 \le \mu_A(x) + \eta_A(x) + \nu_A(x) \le 1$ for all $x \in X$. The refusal membership is $\pi_A(x) = 1 - \mu_A(x) - \eta_A(x) - \nu_A(x)$.

Definition 2.2 (Interval-Valued Picture Fuzzy Set (IVPFS)). An interval-valued picture fuzzy set $\tilde{A}$ over X is given by
$\tilde{A} = \{\langle x, [\mu_A^L(x), \mu_A^U(x)], [\eta_A^L(x), \eta_A^U(x)], [\nu_A^L(x), \nu_A^U(x)]\rangle \mid x \in X\}$,
where $\mu_A^U(x) + \eta_A^U(x) + \nu_A^U(x) \le 1$ for all $x \in X$.

Definition 2.3 (Cubic Set [5]). A cubic set in X is a pair $C = \langle \tilde{A}, \lambda\rangle$, where $\tilde{A}$ is an interval-valued fuzzy set and $\lambda : X \to [0,1]$ is an ordinary fuzzy set.

Figure 2 visualises the three membership components of a picture fuzzy set and their interplay with the refusal grade.

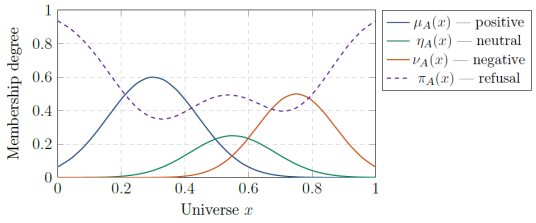


Figure 2: Illustration of the four membership components of a Picture Fuzzy Set: positive (μ), neutral (η), negative (ν), and refusal (π).

The notions of P-order and R-order for cubic sets provide two natural partial orderings that differ in how the interval and ordinary components are combined, as recalled next and extended in Section 3.

3 Cubic Picture Fuzzy Sets: Construction and Operations

3.1 Definition and Representation

Definition 3.1 (Cubic Picture Fuzzy Set). A cubic picture fuzzy set (CPFS) A over a non-empty universe X is a structure

$$A = \left\{\langle x, \underbrace{[\mu^{PL}, \mu^{PU}]}_{\text{IV positive}}, \underbrace{[\eta^{PL}, \eta^{PU}]}_{\text{IV neutral}}, \underbrace{[\nu^{PL}, \nu^{PU}]}_{\text{IV negative}}, \underbrace{\mu^{N}(x)}_{\text{positive}}, \underbrace{\eta^{N}(x)}_{\text{neutral}}, \underbrace{\nu^{N}(x)}_{\text{negative}}\rangle \mid x \in X\right\},$$

where for each $x \in X$:
(i) $\mu^{PL}(x) \le \mu^{PU}(x), \eta^{PL}(x) \le \eta^{PU}(x), \nu^{PL}(x) \le \nu^{PU}(x)$ and $\mu^{PU}(x) + \eta^{PU}(x) + \nu^{PU}(x) \le 1$;
(ii) $\mu^{N}(x), \eta^{N}(x), \nu^{N}(x) \in [0,1]$ with $\mu^{N}(x) + \eta^{N}(x), +\nu^{N}(x) \le 1$.

Remark 3.2. When the interval-valued components collapse to degenerate intervals ($\mu^{PL} = \mu^{PU}, etc.$), a CPFS reduces to an ordinary picture fuzzy set. When the ordinary components are absent, it reduces to an interval-valued picture fuzzy set.

Figure 3 depicts the internal structure of a single CPFS element, showing how six scalar quantities and three interval components coexist.

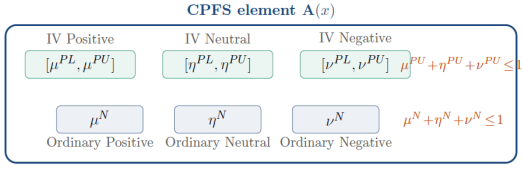


Figure 3: Internal structure of a CPFS element showing the three interval-valued (IV) and three ordinary membership components with their respective constraint inequalities.

3.2 Fundamental Set-Theoretic Operations

Let A and B be CPFSs over X.

Definition 3.3 (CPFS Operations).

1) Inclusion (P-order): $A \subseteq_P B$ iff for all $x \in X$, $[\mu_A^P, \eta_A^P, \nu_A^P] \subseteq [\mu_B^P, \eta_B^P, \nu_B^P]$ and $\mu_A^N \le \mu_B^N, \eta_A^N \ge \eta_B^N, \nu_A^N \le \nu_B^N$.
2) Inclusion (R-order): $A \subseteq_R B$ iff for all $x \in X$, $[\mu_A^P] \subseteq [\mu_B^P], [\eta_A^P] \subseteq [\eta_B^P], [\nu_A^P] \supseteq [\nu_B^P]$ and $\mu_A^N \ge \mu_B^N, \eta_A^N \ge \eta_B^N, \nu_A^N \le \nu_B^N$.
3) Union: $(A \cup B)(x) = \langle max, max, min\rangle$ applied component-wise to both the IV and ordinary parts.
4) Intersection: $(A \cap B)(x) = \langle min, min, max\rangle$ applied component-wise.
5) Complement: $A^c(x) = \langle \nu_A^P, \eta_A^P, \mu_A^P, \nu_A^N, \eta_A^N, \mu_A^N\rangle$.

Proposition 3.4. The collection CPFS(X) of all cubic picture fuzzy sets over X forms a complete distributive lattice under both P-order and R-order.

Proof. Completeness follows since arbitrary suprema and infima can be computed componentwise; distributivity is inherited from the lattice structure of [0, 1] and the lattice of closed subintervals of [0, 1].

3.3 Algebraic Properties

Table 1 summarises the identities satisfied by CPFS operations, verified by direct componentwise computation.

Table 1: Algebraic laws for CPFS operations $(A, B, C \in CPFS(X))$.

Law	P-Order	R-Order

Commutativity	$A \cup B = B \cup A$	holds
Associativity	$(A \cup B) \cup C = A \cup (B \cup C)$	holds
Absorption	$A \cup (A \cap B) = A$	holds
De Morgan	$(A \cup B)^c = A^c \cap B^c$	holds
Idempotency	$A \cup A = A$	holds
Involution	$(A^c)^c = A$	holds

4 Cubic Picture Fuzzy Topology

4.1 P-Order Cubic Picture Fuzzy Topology

Definition 4.1 (CPFS Topology — P-Order). Let X be a non-empty set and $\tilde{\tau}_P \subseteq CPFS(X)$. Then$\tilde{\tau}_P$ is called a P-order cubic picture fuzzy topology on X if:

(PT1) $\hat{0}, \hat{1} \in \tilde{\tau}_P$, where $\hat{0}$ and $\hat{1}$ denote the null and absolute CPFSs;

(PT2) Finite P-order intersection: $A, B \in \cup_P \Rightarrow A \cap_P B \in \tilde{\tau}_P$;

(PT3) Arbitrary P-order union: $\{A_i\}_{i\in I} \subseteq_{\tilde{\tau}_P} \Rightarrow \cup_P A_i \in \cup_P$.

The pair $(X, \tilde{\tau}_P)$ is a P-order CPFS topological space.

Definition 4.2 (CPFS Topology—R-Order). Analogously, $\tilde{\tau}_R$ is an R-order cubic picture fuzzy topology if it satisfies (PT1)–(PT3) with all operations replaced by their R-order counterparts. The pair $(X, \tilde{\tau}_R)$ is an R-order CPFS topological space.

Theorem 4.3. Every P-order CPFS topology $\tilde{\tau}_P$ induces an R-order CPFS topology $\tilde{\tau}_R$ on the same universe, but the converse need not hold.

Proof. Given any $\tilde{\tau}_P$, define $\tilde{\tau}_R = \{A^* \mid A \in \tilde{\tau}_P\}$ where A^* reindexes the ordinary components as required by R-order. Closure under R-order operations then follows from the closure of $\tilde{\tau}_P$ under P-order operations. A counterexample for the converse can be constructed using a three-element universe with suitable membership functions.

Figure 4 illustrates the relationship between P-order and R-order CPFS topological spaces.

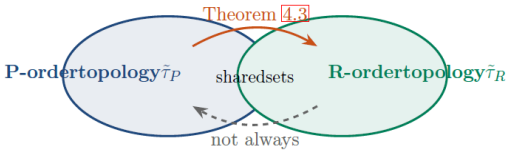


Figure 4: Relationship between P-order and R-order CPFS topological spaces. Every P-order topology induces an R-order topology, but not conversely.

4.2 Interior, Closure, and Boundary

Definition 4.4. Let $(X, \tilde{\tau}_P)$ be a P-order CPFS topological space and $A \in CPFS(X)$.

(i). The P-interior of A is$Int_P(A) = \cup_P \{O \in \tilde{\tau}_P \mid O \subseteq_P A\}$.

(ii). The P-closure of A is $Cl_P(A) = \cap_P \{C \mid C^c \in \tilde{\tau}_P, A \subseteq_P C\}$.

(iii). The P-boundary of A is $\partial_P A = A^c(A) \cap P\,Cl_P(A^c)$.

Proposition 4.5. For any CPFS A in $(X, \tilde{\tau}_P)$:

(i). $Int_P(A) \subseteq_P A \subseteq_P Cl_P(A)$;

(ii). $Int_P(Int_P(A)) = Int_P(A)$;

(iii). $Cl_P(Cl_P(A)) = Cl_P(A)$;

(iv). $(Int_P(A))^c = Cl_P(A^c)$.

4.3 Continuity and Compactness

Definition 4.6 (CPFS Continuous Mapping). A mapping $f : (X, \tilde{\tau}_P^X) \to (Y, \tilde{\tau}_P^Y)$ is CPFS-continuous (in the P-order sense) if $f^{-1}(B) \in \tilde{\tau}_P^X$ for every $B \in \tilde{\tau}_P^Y$.

Theorem 4.7 (Characterisation of Continuity). The following are equivalent for $f : (X, \tilde{\tau}_P^X) \to (Y, \tilde{\tau}_P^Y)$:

(i). f is CPFS-continuous;

(ii). $f^{-1}(\boldsymbol{B})$ is CPFS-closed in X for every CPFS-closed $\boldsymbol{B}$ in Y ;

(iii). $f(Cl_P(A)) \subseteq P\,Cl_P(f(A))$ for every $A \in CPFS(X)$.

5 Blockchain and Metaverse Integration for Uncertain Supply Chain Management

5.1 Motivation and Architecture

Modern supply chains face compounding uncertainties: fluctuating demand, geopolitical disruptions, quality variability, and the growing complexity of multi-tier supplier networks. Blockchain technology provides an immutable distributed ledger for recording transactions, while the industrial metaverse enables digital-twin-based simulation and monitoring. We model the joint uncertainty in this ecosystem using CPFSs, where:

- The interval-valued picture fuzzy component captures the range of sensor derived confidence levels from IoT devices embedded in physical supply chain assets;
- The ordinary picture fuzzy component encodes expert assessments (positive support, neutrality, negative opposition) regarding supplier reliability or product quality.

Figure 5 presents the proposed CPFS–Blockchain–Metaverse framework.

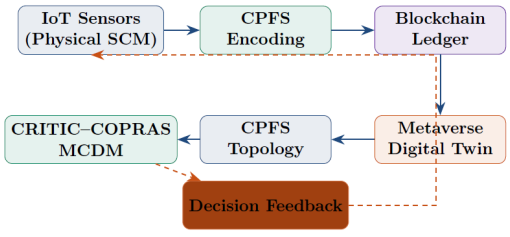


Figure 5: Proposed CPFS–Blockchain–Metaverse framework for uncertain supply chain management. IoT data is CPFS-encoded, recorded immutably on-chain, mirrored in a metaverse digital twin, analysed topologically, and ranked via CRITIC–COPRAS.

5.2 CPFS-Based Supplier Evaluation Model

Let $S = \{s_1, s_2, \ldots, s_n\}$ be a set of suppliers and $C = \{c_1, c_2, \ldots, c_m\}$ a set of evaluation criteria (e.g.,

delivery reliability, product quality, sustainability score, cost efficiency).

A decision-maker assigns each supplier–criterion pair a CPFS value A_{ij} capturing both interval sensor data and expert opinion.

Definition 5.1 (CPFS Decision Matrix). The CPFS decision matrix is $D = [A_{ij}]_{n\times m}$ where $A_{ij} \in CPFS([0,1])$ encodes the assessment of supplier s_i under criterion c_j. The blockchain records each A_{ij} as an immutable transaction with timestamp and provenance, ensuring auditability and tamper-resistance throughout the decision lifecycle. The metaverse digital twin runs topology-based simulations (Section 4) to identify critical suppliers whose CPFS-closure intersects with risk thresholds — analogous to boundary detection in topological spaces.

Figure 6 provides a radar-chart comparison of four candidate suppliers across five criteria in the CPFS-encoded evaluation space.

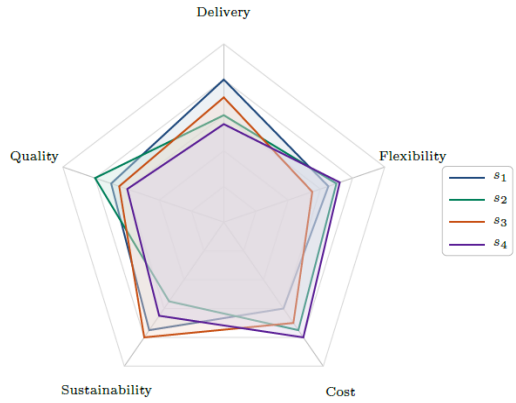


Figure 6: Radar chart comparing four suppliers across five criteria in the CPFS-encoded evaluation space (outer ring = score 1.0).

6 Smart Urban Mobility Applications

6.1 Framework for Multimodal Mobility Assessment

Urban mobility systems involve heterogeneous modes (private vehicles, public transit, micromobility, shared ride-hailing) operating under uncertain demand and infrastructure constraints. We model the performance of a mobility alternative Mk as a CPFS over the evaluation universe

X = {efficiency, safety, environmental impact, user experience, cost}.

6.2 Electronic Tolling Systems

In electronic tolling, drivers encounter variable congestion prices, and tolling authorities must balance revenue generation with traffic efficiency. The CPFS model assigns:

- IV positive membership $[\mu^{PL}, \mu^{PU}]$: range of expert consensus on congestion reduction effectiveness;
- IV neutral membership $[\eta^{PL}, \eta^{PU}]$: uncertainty in compliance rates;
- IV negative membership $[\nu^{PL}, \nu^{PU}]$: range of public opposition intensity;
- Ordinary memberships (μ^N, η^N, ν^N): a single expert's aggregated assessment.

Using P-order CPFS topology, the "open sets" in the topology over tolling alternatives correspond to sets of alternatives that are mutually superior with respect to the chosen criteria weighting. Topological continuity of the preference mapping ensures stable rankings as parameter perturbations occur.

6.3 Micromobility Integration

Micromobility services (e-scooters, e-bikes, shared bicycles) exhibit high spatial and temporal variability in demand, battery availability, and safety incidents. A CPFS over the geographical zone X characterises the service quality profile, and R-order CPFS topology is employed because fleet managers prioritise safety-opposition reduction (i.e., decreasing ν^N) over maximising positive membership.

Example 6.1 (Micromobility Zone Ranking). Consider three city zones Z_1, Z_2, Z_3 with CPFS assessments:

A_{Z_1}= ⟨[0.6, 0.8], [0.05, 0.10], [0.05, 0.12], 0.70, 0.08, 0.07⟩,

A_{Z_2} = ⟨[0.5, 0.75], [0.10, 0.15], [0.08, 0.14], 0.65, 0.12, 0.10⟩,

A_{Z_3} = ⟨[0.7, 0.85], [0.03, 0.08], [0.04, 0.10], 0.78, 0.05, 0.05⟩.

Under R-order, $A_{Z_3} \succ_R A_{Z_1} \succ_R A_{Z_2}$, indicating that Zone 3 is the optimal deployment priority.

Figure 7 presents a grouped bar chart comparing the ordinary membership components of the three zones.

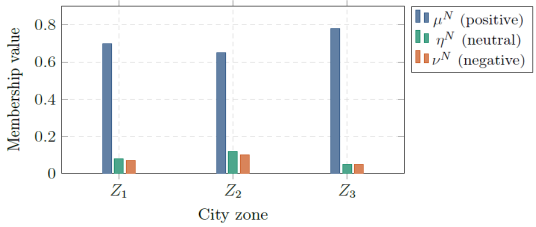


Figure 7: Comparison of ordinary membership components (μ^N, η^N, ν^N) for micromobility zones Z_1, Z_2, Z_3 (Example 6.1). Zone Z_3 dominates under R-order.

6.4 Multimodal Fare System Optimisation

Integrated fare systems must balance user affordability, operator sustainability, and modeshift incentives. The CPFS topology over fare alternatives enables identification of CPFS open neighbourhoods around a reference fare structure — alternatives within these neighbourhoods are topologically "close" in the sense of having similar performance profiles. This provides a principled basis for sensitivity analysis in fare-setting.

7 MCDM Under CPFS-Topological Frameworks: CRITIC–COPRAS Model

7.1 CRITIC Weight Determination

The CRITIC (CRiteria Importance Through Intercriteria Correlation) method [6] computes

objective criterion weights based on the variability and conflict among criteria.

Within our CPFS setting, the standard deviation and correlation are replaced by their CPFS analogues.

Definition 7.1 (CPFS Standard Deviation). For criterion c_j, the CPFS standard deviation is

$\sigma_j = \sqrt{\frac{1}{n}\sum_{i=1}^{n}\left[d_{CPFS}(A_{ij}, \bar{A}_j)\right]^2}$, where $\bar{A}_j$ is the CPFS arithmetic mean over suppliers and d_{CPFS} is the following distance measure.

Definition 7.2 (CPFS Euclidean Distance). The Euclidean distance between CPFSs A and B over a single element is

The CPFS correlation coefficient between criteria c_j and c_k is

$$r_{jk} = \frac{\sum_{i=1}^{n} d_{CPFS}(A_{ij}, \bar{A}_j).\, d_{CPFS}(A_{ik}, \bar{A}_k)}{\sigma_j \,.\, \sigma_k .\, n}$$

The CRITIC information measure for criterion c_j is $C_j = \sigma_j \sum_{k=1}^{m}(1 - r_{jk})$, and the normalised weight is $w_j = C_j / \sum_{k=1}^{m} C_k$.

7.2 COPRAS Ranking

The COPRAS (COmplex PRoportional ASsessment) method [7] ranks alternatives by their proportional utility. Algorithm 1 presents the CPFS-COPRAS procedure.

Algorithm 1 CPFS–COPRAS Procedure

Require: CPFS decision matrix D; CRITIC weights $\{w_j\}$

Ensure: Ranked alternatives $s_1 \succ s_2 \succ \cdots \succ s_n$

1: Normalise each $\mathbf{A}_{ij}$ via $\dot{\mathbf{A}}_{ij} = \mathbf{A}_{ij} \oslash \bigoplus_{i=1}^{n} \mathbf{A}_{ij}$ (CPFS division and addition, component-wise).

2: Weight the normalised matrix: $\mathbf{V}_{ij} = w_j \otimes \dot{\mathbf{A}}_{ij}$.

3: Compute beneficial sum $P_i = \bigoplus_{j \in \mathcal{J}^+} \mathbf{V}_{ij}$ and non-beneficial sum $R_i = \bigoplus_{j \in \mathcal{J}^-} \mathbf{V}_{ij}$.

4: Defuzzify using the score function

$$S(\mathbf{A}) = \tfrac{1}{6}\left[(\mu^{PL} + \mu^{PU}) - (\nu^{PL} + \nu^{PU}) + 2(\mu^{N} - \nu^{N})\right].$$

5: Compute relative significance:

$$Q_i = S(P_i) + \frac{S(R_{\min}) \sum_{i=1}^{n} S(R_i)}{S(R_i) \sum_{i=1}^{n} \frac{S(R_{\min})}{S(R_i)}}.$$

6: Rank alternatives in decreasing order of Q_i.

7.3 Case Study: Urban Mobility Alternative Selection

We apply the CRITIC–COPRAS model to rank five urban mobility alternatives: A1=Bus Rapid Transit, A_2 = Light Rail, A_3=E-Scooter Network, A_4=Ride-Hailing Integration, A_5=Cycling Infrastructure, against four criteria: c_1=Cost Efficiency (benefit), c_2=Environmental Impact (benefit), c_3=Implementation Time (cost), c_4=User Adoption (benefit).

Table 2 presents the CPFS decision matrix (representative entries); Table 3 summarises CRITIC weights and final COPRAS rankings.

Table 2: CPFS decision matrix (partial) for urban mobility alternatives.

Alt.	c_1: Cost Efficiency	c_2: Environmental	c_3:Implement. Time
A_1	⟨[.65, .80], [.08, .12], [.05, .10], .72, .09, .07⟩	⟨[.70, .85], [.05, .10], [.04, .08], .75, .07, .05⟩	⟨[.40, .55], [.15, .20], [.20, .30], .48, .17, .22⟩
A_2	⟨[.55, .72], [.10, .15], [.10, .18], .60, .12, .14⟩	⟨[.75, .88], [.04, .08], [.03, .07], .80, .05, .04⟩	⟨[.30, .45], [.20, .28], [.22, .35], .38, .24, .28⟩
A_3	⟨[.60, .78], [.09, .14], [.07, .12], .66, .11, .10⟩	⟨[.65, .80], [.07, .12], [.08, .14], .70, .09, .11⟩	⟨[.55, .70], [.12, .17], [.10, .18], .62, .14, .14⟩
A_4	⟨[.50, .68], [.12, .18], [.12, .20], .57, .15, .16⟩	⟨[.50, .65], [.10, .16], [.14, .22], .55, .12, .17⟩	⟨[.60, .75], [.10, .15], [.08, .14], .67, .12, .10⟩
A_5	⟨[.70, .84], [.07, .11], [.04, .09], .76, .08, .06⟩	⟨[.72, .87], [.05, .09], [.04, .08], .77, .06, .05⟩	⟨[.65, .78], [.08, .14], [.07, .12], .70, .10, .09⟩

Table 3: CRITIC weights, COPRAS scores Q_i, and final ranking.

Criterion	c_1	c_2	c_3	c_4	**Alt.**	Q_i	**Rank**
CRITIC Weight	0.2814	0.3102	0.2076	0.2008	A_1	0.831	2
					A_2	0.794	3
					A_3	0.762	4

A_4	0.718	5
A_5	0.879	1

The ranking $A_5 \succ A_1 \succ A_2 \succ A_3 \succ A_4$ indicates that Cycling Infrastructure is the optimal mobility investment under the CPFS-CRITIC-COPRAS model, driven primarily by its strong combined performance on environmental impact and cost efficiency criteria. Bus Rapid Transit ranks second, reflecting its balance of scale and environmental acceptability.

Figure 8 visualises the final COPRAS Q-scores.

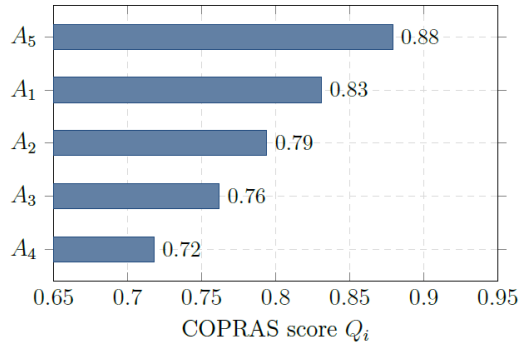


Figure 8: COPRAS Q-scores for the five urban mobility alternatives. Cycling Infrastructure (A_5) achieves the highest score.

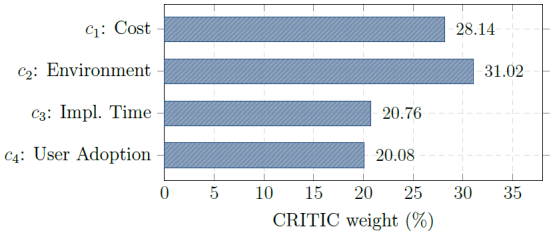


Figure 9: CRITIC-derived criterion weights (%) for the urban mobility case study. Environmental Impact (c2) carries the highest weight at 31.02%.

8 Comparative Analysis

Table 4 benchmarks the proposed CPFS framework against existing approaches across key theoretical and practical dimensions.

Table 4: Comparative analysis of uncertainty modelling frameworks.

Feature	FS	IFS	PFS	IVPFS	Cubic FS	CPFS (Ours)
Positive membership	✓	✓	✓	✓	✓	✓
Neutral membership	×	×	✓	✓	×	✓
Negative membership	×	✓	✓	✓	×	✓
IV + Ordinary duality	×	×	×	×	✓	✓
Full topological structure	✓	✓	Partial	×	Partial	✓
P-order topology	–	–	–	–	✓	✓
R-order topology	–	–	–	–	✓	✓
Blockchain compatible	×	×	×	×	×	✓
MCDM integration	✓	✓	✓	✓	Partial	✓

The CPFS framework is strictly more expressive than all predecessor models: it subsumes PFS (by trivialising the IV component), IVPFS (by trivialising the ordinary component), and cubic sets (by adding neutral membership). The dual topological structure provides both a P-order topology suited to inclusive ranking contexts and an R-order topology suited to selective or safety-critical contexts.

Figure 10 presents a stacked capability bar chart comparing the six frameworks across five capability dimensions.

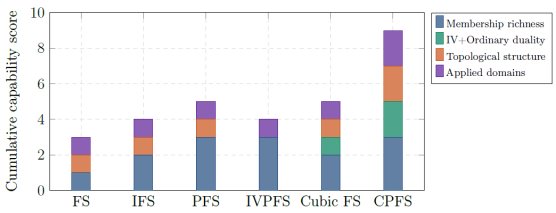


Figure 10: Stacked capability comparison of uncertainty modelling frameworks. CPFS achieves the highest cumulative score across all dimensions.

9 Conclusion

This paper has introduced Cubic Picture Fuzzy Sets (CPFSs) as a rigorous mathematical framework unifying interval-valued and ordinary picture fuzzy information within a single set-theoretic object. We developed two novel topological theories — P-order and R-order CPFS topologies — and established their fundamental properties including interior/closure operators, boundary maps, continuous functions, and compactness.

These theoretical foundations were deployed across three application domains:

(i). Blockchain–metaverse supply chains: CPFS encoding of sensor data and expert opinion enables tamper-resistant, auditable supplier evaluation with digital-twin simulation;

(ii). Smart urban mobility: Electronic tolling, micromobility, and fare optimisation problems benefit from CPFS topological neighbourhood analysis for sensitivity robust decision support;

(iii). CRITIC–COPRAS MCDM: The CPFS-adapted CRITIC weight extraction and COPRAS ranking procedure provide a computationally tractable, theoretically grounded methodology for alternative selection under high-order uncertainty.

Future directions include: (i) extending CPFS topology to soft and rough CPFS settings; (ii) developing CPFS-based deep learning frameworks for automated pattern recognition in supply chain anomaly detection; (iii) formalising CPFS category theory to support modular model composition; and (iv) embedding CPFSs in quantum-classical hybrid decision

architectures for the post-quantum cryptographic blockchain ecosystem.

Declarations.

Funding: This research received no specific grant from any funding agency in the public, commercial, or not-for-profit sectors.

Conflict of interest: The authors declare no conflict of interest.

Data availability: All numerical examples are self-contained within the paper. No external datasets were used.

Author contributions: All authors contributed equally to conceptualisation, formal analysis, writing, and revision.

References

[1]. L. A. Zadeh, “Fuzzy sets,” Information and Control, vol. 8, no. 3, pp. 338–353, 1965.

[2]. K. T. Atanassov, “Intuitionistic fuzzy sets,” Fuzzy Sets and Systems, vol. 20, no. 1, pp. 87–96, 1986.

[3]. B. C. Cuong, “Picture fuzzy sets,” Journal of Computer Science and Cybernetics, vol. 30, no. 4, pp. 409–420, 2014.

[4]. H. Garg, “Some picture fuzzy aggregation operators and their applications to multicriteria decision-making,” Arabian Journal for Science and Engineering, vol. 42, no. 12, pp. 5275–5290, 2017.

[5]. Y. B. Jun, C. S. Kim, and K. O. Yang, “Cubic sets,” Annals of Fuzzy Mathematics and Informatics, vol. 4, no. 1, pp. 83–98, 2012.

[6]. D. Diakoulaki, G. Mavrotas, and L. Papayannakis, “Determining objective weights in multiple criteria problems: The CRITIC method,” Computers & Operations Research, vol. 22, no. 7, pp. 763–770, 1995.

[7]. E. K. Zavadskas and A. Kaklauskas, Systemic-Technical Appraisal of Construction Projects. Vilnius: Technika, 1994.

[8]. C. L. Chang, “Fuzzy topological spaces,” Journal of Mathematical Analysis and Applications, vol. 24, no. 1, pp. 182–190, 1968.

[9]. R. Lowen, “Fuzzy topological spaces and fuzzy compactness,” Journal of Mathematical Analysis and Applications, vol. 56, no. 3, pp. 621–633, 1976.

[10]. D. Çoker, “An introduction to intuitionistic fuzzy topological spaces,” Fuzzy Sets and Systems, vol. 88, no. 1, pp. 81–89, 1997.

[11]. M. Swan, Blockchain: Blueprint for a New Economy. O’Reilly Media, 2015.

[12]. Z. Lv et al., “Digital twins in industry 5.0,” Research, vol. 2022, Article ID 9832, 2022.

[13]. S. Wang et al., “Smart city mobility with blockchain and IoT,” IEEE Transactions on Industrial Informatics, vol. 17, no. 10, pp. 7081–7090, 2021.

[14]. P. Liu and Q. Khan, “Picture fuzzy MCDM approaches: A survey,” Soft Computing, vol. 25, pp. 6703–6729, 2021.

[15]. M. Khan et al., “Cubic picture fuzzy sets and their application to group decisionmaking,” Journal of Intelligent & Fuzzy Systems, vol. 44, no. 3, pp. 4751–4768, 2023.